

HBT interferometry with quantum transport of the interfering pair

Li-Li Yu¹, Wei-Ning Zhang^{1,2}, and Cheuk-Yin Wong^{2,3}

¹*Department of Physics, Harbin Institute of Technology, Harbin, Heilongjiang 150006, P. R. China*

²*School of Physics and Optoelectronic Technology,*

Dalian University of Technology, Dalian, Liaoning 116024, P. R. China

³*Physics Division, Oak Ridge National Laboratory, Oak Ridge, TN 37831, U.S.A.*

(Dated: November 9, 2018)

In the late stage of the evolution of a pion system in high-energy heavy-ion collisions when pions undergo multiple scatterings, the quantum transport of the interfering pair of identical pions plays an important role in determining the characteristics of the Hanbury-Brown-Twiss (HBT) interference. We study the quantum transport of the interfering pair using the path-integral method, in which the evolution of the bulk matter is described by relativistic hydrodynamics while the paths of the two interfering pions by test particles following the fluid positions and velocity fields. We investigate in addition the effects of secondary pion sources from particle decays, for nuclear collisions at AGS and RHIC energies. We find that quantum transport of the interfering pair leads to HBT radii close to those for the chemical freeze-out configuration. Particle decays however lead to HBT radii greater than those for the chemical freeze-out configuration. As a consequence, the combined effects give rise to HBT radii between those extracted from the chemical freeze-out configuration and the thermal freeze-out configuration. Proper quantum treatments of the interfering pairs in HBT calculations at the pion multiple scattering stage are important for our understanding of the characteristics of HBT interferometry in heavy-ion collisions.

PACS numbers: 25.75.-q, 25.75.Gz, 25.75.Nq

I. INTRODUCTION

Two-pion Hanbury-Brown-Twiss (HBT) interferometry has been widely used in high energy heavy ion collisions to study the space-time geometry of particle-emitting sources [1, 2, 3, 4]. As is well known, the HBT interference occurs for a chaotic source and is absent for a coherence source [5]. It is therefore important to identify the proper “chaotic” source to compare theoretical results with experimental measurements.

Usual theoretical treatments of the HBT problem argue that the collisions in the thermalisation of pions at the late stage of the evolution behaves as collisions of classical particles in a chaotic system, and these chaotic collisions will lead to a chaotic thermal freeze-out configuration. According to this argument, the thermal freeze-out configuration should therefore be the proper “chaotic” source in HBT measurements and the HBT radii are expected to increase substantially with increasing collision energies. However, experimental data indicate that there are only relatively small changes of HBT radii when the energy increases from AGS, SPS, to RHIC energies [6, 7, 8, 9, 10, 11, 12, 13].

As the proper identification of the HBT “chaotic” pion source is crucial to the understanding of the phenomenon, it is necessary to examine the nature of the pion source during the late stage of its evolution. One envisages that as the pion system cools down, the kinetic energies of the pions may initially be quite high so that chemical reactions among pions can take place, leading to the conversion of pions into kaons (and vice versa). These chemical reactions will lower their intensities significantly when the temperature decreases below a limit. The system will undergo chemical freeze-out at which the yield ratios of dominant particles are nearly fixed. Before chemical freeze-out, the identities of the particles are still in a state of flux. Therefore, it is reasonable to take the chemical freeze-out configuration to be the initial “chaotic” pion source for the purpose of studying the HBT interference.

The “chaotic” source is however not a static source from which the pair of interfering identical pions are emitted and detected. The chaotic source continues to evolve and the pair of pions must follow the evolution from the chemical freeze-out configuration to the state of thermal freeze-out. Only at the state of thermal freeze-out can the pair of pions be free of interactions and can be considered “emitted” to the detector. How the pair of pions propagate from the initial chemical freeze-out point to the thermal freeze-out point will affect the characteristics of HBT interference and will be the subject of the present investigation.

At temperatures below the chemical freeze-out temperature, pions undergo multiple scattering with the medium particles. The scattering can be elastic or inelastic. Thermalisation takes place until the temperature reach the thermal freeze-out limit, at which the shapes of momentum distributions of final particles are determined [14, 15, 16]. Thus, the last stage of the evolution of the pion system makes a transition from a chemical-reaction dominating epoch before chemical freeze-out to a multiple scattering dominating epoch between chemical freeze-out and thermal freeze-out.

In the usual treatment of the HBT problem, the last stage of multiple scattering is envisaged as random cascades of

classical binary collisions and the spatial configuration of the system after these random binary collisions will continue to be chaotic in the newly-evolved and expanded configuration. Such a viewpoint may indeed be valid for some other considerations of the state of the system, it is nonetheless inadequate for the HBT interference for a pair of identical particles. It is important to note that the HBT interference phenomenon is quantum mechanical in nature, arising from the interference of pairs of identical pions traveling through different history paths to reach two detectors. The propagation of a pair of pions which undergo multiple scattering with the medium at the late stage of the evolution should be treated quantum mechanically [17, 18, 19, 20, 21, 22].

Upon carrying out such an investigation for a pair of test particles in the path-integral method, it was previously realized that the collisions of the pion with medium particles at the late stage of the evolution lead to the accumulation of the phases of the pion wave functions. The real parts of these phase shifts of the pair tend to cancel while the imaginary part leads to an absorption in the two-pion interferometry [17, 18, 19, 20]. As a consequence, the effective source size is not necessarily that of the newly-evolved spatial configuration as in thermal freeze-out, but may be significantly smaller. We would like to demonstrate such an effect explicitly here by assuming a chaotic source at chemical freeze-out and by following the quantum transport of the interfering pair, using the path integral method for which the pions need not follow straight-line trajectories. For such a study we use relativistic hydrodynamics to describe the evolution of the bulk matter while the paths of the two interfering pions are described by test particles following the hydrodynamical fluid positions and velocity fields. Alternative descriptions of particle emission using different view points have also been presented previously [21, 22, 23].

In following the evolution of pairs of identical pions, there are additional complications. Pions are produced not only directly at chemical freeze-out but also indirectly by particle decays as secondary pions during the period from chemical freeze-out to thermal freeze-out. It is necessary to include these secondary pions in our HBT calculations. The HBT radius for the evolving source will reflect not only the geometry of the source at a configuration close to the chemical freeze-out configuration but the effects of these secondary sources. Because the secondary sources are different for AGS collisions and RHIC collisions, we shall study the effects of particle decays for collisions at both AGS and RHIC energies. As the present investigation is for demonstration purposes, we shall limit our attention on spherical geometry. To assist future investigations utilizing quantum transport of the interfering pair, we present a detail description of the procedures how this quantum transport is carried out in the path integral method.

The paper is organized as follows. In Sec. II, we give a brief review of equations of relativistic hydrodynamics and discuss the equations of state for sources produced in collisions at AGS and RHIC energies. We also discuss the particle production conditions in this section. In Sec. III, we review the two-pion HBT correlation function in quantum probability amplitudes in a path-integral formalism. We examine the HBT radii for the evolving source, and investigate the effects of particle decay and multiple scattering on HBT radii both for AGS and RHIC energies. Finally, a summary and discussion are presented in Sec. IV.

II. EVOLUTION OF THE PARTICLE SOURCE

As a completely quantum mechanical description of the evolution of the full system is not within reach, we shall study the evolution of the bulk strongly-interacting matter by relativistic hydrodynamics, which has been quite successful in high-energy heavy-ion collisions. We shall then examine the interference of the pair of pions by following their trajectories as test particles in the fluid after the chemical freeze-out.

A. Equations of relativistic hydrodynamics

In relativistic hydrodynamics, the dynamics of the strongly-interacting fluid is defined by local conservations of energy-momentum and net charges [24, 25, 26]. In our model calculations we use conservations of energy-momentum, net baryon number, and entropy of the system. The continuity equations of these conservations are [24, 25, 26]

$$\partial_\mu T^{\mu\nu}(x) = 0, \quad (1)$$

$$\partial_\mu j_b^\mu(x) = 0, \quad (2)$$

$$\partial_\mu j_s^\mu(x) = 0, \quad (3)$$

where x is the space-time coordinate of a thermalize fluid element in the source center-of-mass frame, $T^{\mu\nu}(x)$ is the energy momentum tensor of the element, $j_b^\mu(x) = n_b(x)u^\mu$ and $j_s^\mu(x) = s(x)u^\mu$ are the four-current-density of baryon

and entropy (n_b and s are baryon density and entropy density), and $u^\mu = \gamma(1, \mathbf{v})$ is the 4-velocity of the fluid element. The energy momentum tensor can be expressed as [24, 25, 26, 27]

$$T^{\mu\nu}(x) = [\epsilon(x) + p(x)]u^\mu(x)u^\nu(x) - p(x)g^{\mu\nu}, \quad (4)$$

where p and ϵ are the pressure and energy density of the fluid element, and $g^{\mu\nu}$ is the metric tensor.

From the local conservations Eqs. (1)–(3), one can get the equations of motion for spherical geometry as [24, 25]

$$\partial_t E + \partial_r[(E + p)v] = -\frac{2v}{r}(E + p), \quad (5)$$

$$\partial_t M + \partial_r(Mv + p) = -\frac{2v}{r}M, \quad (6)$$

$$\partial_t N_b + \partial_r(N_b v) = -\frac{2v}{r}N_b, \quad (7)$$

$$\partial_t N_s + \partial_r(N_s v) = -\frac{2v}{r}N_s, \quad (8)$$

where $E \equiv T^{00}$, $M \equiv T^{0r}$, $N_b = n_b \gamma$, $N_s = s \gamma$. Using the HALE scheme [28, 29] and Sod's operator splitting method [30], one can obtain the solutions of Eqs. (5)–(8) [20, 24, 25, 31], after knowing the initial conditions and equations of state. In our calculations, we assume that the initial systems are distributed uniformly within a sphere with radius r_0 and have zero initial velocity. The grid spacing and time step in the calculations are taken as $\Delta x = 0.04r_0$ and $\Delta t = 0.99\Delta x$.

B. Equation of state

In the equations of motion (5)–(8), there are ϵ , p , v , n_b , and s five unknown functions. In order to obtain the solution of the equations of motion, we need an equation of state (EOS), $p(\epsilon, n_b, s)$, which gives a relation for p , ϵ , n_b , and s [25].

1. EOS for system at AGS energies

At AGS energies, we use a mixed perfect gas of hadrons to describe the particle-emitting source. The number density, energy density, pressure, and entropy density of the particle species i for a thermalized fluid element can be expressed in the fluid element local frame in terms of temperature $T(x)$ and chemical potential $\mu_i(x)$ as

$$n_i = \frac{4\pi g_i}{(2\pi)^3} \int_{m_i}^{\infty} f_i E \sqrt{E^2 - m_i^2} dE, \quad (9)$$

$$\epsilon_i = \frac{4\pi g_i}{(2\pi)^3} \int_{m_i}^{\infty} f_i E^2 \sqrt{E^2 - m_i^2} dE, \quad (10)$$

$$p_i = \frac{1}{3} \frac{4\pi g_i}{(2\pi)^3} \int_{m_i}^{\infty} f_i (E^2 - m_i^2)^{3/2} dE, \quad (11)$$

$$s_i = \frac{4\pi g_i}{(2\pi)^3} \int_{m_i}^{\infty} [-f_i \ln f_i \mp (1 \mp f_i) \times \ln(1 \mp f_i)] E \sqrt{E^2 - m_i^2} dE, \quad (12)$$

where

$$f_i = \frac{1}{\exp[(E - \mu_i)/T] \pm 1}, \quad (13)$$

g_i and m_i are the internal freedom and mass of particle species i , and the sign (+) or (-) is for fermions or bosons. The fluid energy density ϵ , pressure p , and entropy density s are the sum of ϵ_i , p_i , and s_i for all particle species considered in the mixed perfect gas, respectively. The baryon density n_b is the sum of n_i for all baryon species in the gas.

For a given set of variable (T, μ_1, μ_2, \dots) , one can obtain the equation of state $p(\epsilon, n_b, s)$ from Eqs. (9)–(12) numerically. Additionally, using HALE scheme to solve equations of fluid dynamics we need the sound velocity of the fluid, $c_s^2 = \partial p / \partial \epsilon$, which can be expressed for the mixed perfect gas as

$$c_s^2 = \sum_i \int_{m_i}^{\infty} f_i (1 \mp f_i) (E^2 - m_i^2)^{3/2} (E - \mu_i) dE \\ \div \sum_i \int_{m_i}^{\infty} \frac{f_i (1 \mp f_i)}{3} \sqrt{E^2 - m_i^2} (E - \mu_i) E^2 dE. \quad (14)$$

2. EOS for system at RHIC energy

At RHIC energy, the system undergoes a transition from QGP phase to hadronic phase. The initial baryon density in the center rapidity region of the collisions is approximately zero because the total number of pions is much greater than the total baryon numbers and there is some tendency of baryon transparency. At zero net baryon density, QCD lattice results suggest the entropy density of the system as a function of temperature as [24, 25, 32, 33]

$$\frac{s(T)}{s_c} = \left(\frac{T}{T_c} \right)^3 \left[1 + \frac{\Theta - 1}{\Theta + 1} \tanh \left(\frac{T - T_c}{\Delta T} \right) \right], \quad (15)$$

where s_c is the entropy density at the transition temperature T_c , ΔT ($0 < \Delta T < 0.1T_c$) is the width of the transition, Θ is a parameter associated with the ratio of the degrees of freedom of the QGP phase to the hadronic phase. For $\Delta T = 0$, the equation of state (15) reduces to the MIT bag equation of state with bag constant $B = (\Theta - 1)T_c s_c / 2(\Theta + 1)$ [24, 25, 34].

For zero net baryon density we only need to solve Eqs. (5), (6), and (8). The thermodynamical relations among p , ϵ , and s in this case are

$$-s dT + dp = 0, \quad (16)$$

$$\epsilon = Ts - p. \quad (17)$$

From these thermodynamical relations and Eq. (15), one can obtain the equation of state $p(\epsilon, s)$ and sound velocity c_s . At the temperature below $(1 - \Delta T)T_c$, the source is in hadronic phase and the equation of state is taken as the mixed perfect gas of hadrons with zero baryon density.

C. Particle sources

How the particle number and its chemical composition may change as the fluid evolves can be described by three different possibilities, some more realistic than others. They are all included here to show various limiting cases. As the equation of state of the fluid depends on particle number and the chemical composition, they also lead to different hydrodynamical evolutions.

1. Partial chemical equilibrium production

As the temperature of the fluid decreases, the kinetic energy for the collision between particles decreases. As a consequence, dominant chemical reactions of converting pions to kaons will lower their intensities and will eventually stop when the temperature decreases below a certain limit. For the problem we are considering, the limiting temperature occurs when the average collision energy at the chemical freeze-out temperature is equal to the threshold for the reaction to change two pions to two kaons. The state of the system when this limit of temperature is reached can be described as the state of chemical freeze-out, when the equilibrium yield ratios of the dominating components (pions and kaons) are frozen.

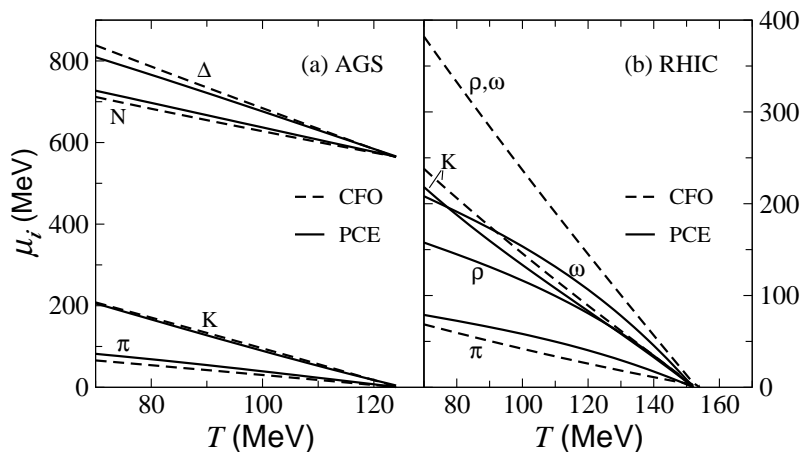


FIG. 1: Chemical potentials of hadrons for CFO production (dotted lines) and PCE production (solid lines) for AGS and RHIC energies.

From the passage of chemical freeze-out to thermal freeze-out, the fluid continues to evolve. Its chemical composition can continue to change as particles can decay into other particles with various life-times. Conversely, the decay product particles can recombine to form parent particles. Some processes with larger cross sections can also equilibrate even below T^{ch} . The chemical composition during this stage is however not in a state of complete chemical equilibrium. We can call it the state of partial chemical equilibrium (PCE). This is the most realistic case when we include the decay and recombination of particles [14, 35]. We follow Hirano and Tsuda [14] to assume that below T^{ch} the chemical potential of particle species i , $\mu_i(T)$, obeys

$$\frac{\bar{n}_i(T, \mu_i)}{s(T, \{\mu_i\})} = \frac{\bar{n}_i(T^{\text{ch}}, \mu_i^{\text{ch}})}{s(T^{\text{ch}}, \{\mu_i^{\text{ch}}\})}, \quad (18)$$

where $\bar{n}_i = n_i + \sum_{j \neq i} \tilde{d}_{j \rightarrow i} n_j$, and $\tilde{d}_{j \rightarrow i}$ is the fraction of excited-state particle species j that decays to the stable particle species i [14, 35].

2. Chemical freeze-out production

For our comparison, it is of interest to examine the less realistic cases when the decay of particles is not considered and other chemical reactions do not take place after chemical freeze-out (CFO). In this case, the chemical composition of the particles are frozen as at the state of chemical freeze-out and all final particles are produced thermally from the source configuration at the chemical freeze-out temperature $T^{\text{ch}} < T_c$. Below T^{ch} all numbers of hadrons are fixed and that the particle number densities obey $\partial_\mu(n_i u^\mu) = 0$. Eq. (18) is changed to [14]

$$\frac{n_i(T, \mu_i)}{s(T, \{\mu_i\})} = \frac{n_i(T^{\text{ch}}, \mu_i^{\text{ch}})}{s(T^{\text{ch}}, \{\mu_i^{\text{ch}}\})}. \quad (19)$$

We can obtain the chemical potential $\mu_i(T)$ as a function of temperature below T^{ch} from Eq. (19), which ensures keeping the number of the hadron i fixed.

Figs. 1(a) and (b) give the chemical potential $\mu_i(T)$ for the sources produced at AGS and RHIC energies, and CFO and PCE modes of production. For the CFO production, the chemical potentials of all particles are calculated from Eq. (19). For the PCE production, the chemical potentials of the stable particles are calculated from Eq. (18), and the chemical potentials of the excited-state particles are obtained from the relations of chemical equilibrium, $\mu_\Delta = \mu_N + \mu_\pi$, $\mu_\rho = 2\mu_\pi$, and $\mu_\omega = 3 \times 0.88\mu_\pi$ [14, 35].

In our model calculations for the source produced in collisions at AGS energies, the initial temperature and baryon chemical potential are taken as 155 MeV and 540 MeV, which correspond to an initial energy density of $\epsilon_0 = 0.56$ GeV/fm³. For simplicity, we only consider N , π , and K as stable particles, and $\Delta(1232)$ as excited-state particle for

the source with finite baryon density. The chemical freeze-out temperature is taken as $0.8T_0 = 124$ MeV, and the corresponding chemical potential is 565 MeV. They are consistent with the freeze-out values obtained from hadronic abundances at CERN/SPS, NBL/AGS, and GSI/SIS [36]. For the source with zero baryon density produced in the collisions at RHIC energy, we take the initial temperature as 250 MeV, which corresponds to an initial energy density of $\epsilon_0 = 4.64$ GeV/fm³. The phase transition temperature T_c and the width of the transition ΔT are taken as 170 MeV and $0.05T_c$. For the chemical freeze-out temperature [14], we take the chemical freeze-out temperature as $0.9T_c = 153$ MeV. We consider π , K , and η as stable particles and take ρ and ω as excited-state particles after the chemical freeze-out. The value of Θ in the equation of state (15) is taken as 5, by consisting the entropy density calculated from Eq. (15) with the result of the entropy density calculated for the mixed perfect gas of hadrons at the chemical freeze-out temperature.

3. Chemical equilibrium up to thermal freeze-out

Finally, we can also examine another less realistic case when chemical equilibrium can be maintained through-out the passage up to thermal freeze-out (TFO), with the emission of particles. Implicit in this scenario is the assumption that all through the hydrodynamical evolution, the kinetic energy for the collision between particles is always large enough to allow chemical reactions to take place to change the chemical composition. Although this may be a good picture for classical fluids when the temperature is comparable to the energy needed for chemical reactions, this may not be as realistic for our case when the kinetic energy in these temperatures is lower than threshold energy for the reactions of two pions converting into two kaons.

For the TFO particle production, the state of chemical freeze-out coincides with the state of thermal freeze-out at T^{th} . For AGS energies, the chemical potentials of π and K are zero and the chemical potentials of N and Δ are the same as the initial baryon chemical potential. For RHIC energy, all final particles have zero chemical potential.

III. TWO-PION INTERFEROMETRY ANALYSIS

A. Path integral formalism of the HBT correlation function

As the identities of particles undergo changes during chemical reactions, the pion source at the moment of chemical freeze-out can be characterized as chaotic in nature, for the purpose of investigating HBT interferometry. The system subsequently expands, its temperature decreases, and its apparent size increases. During the evolution from chemical freeze-out to thermal freeze-out, the dynamics is dominated by multiple scattering of the pions.

It is in the nature of the HBT interference that under the action of multiple scattering after chemical freeze-out, the quantum transport of the interfering pair of pions determines their eventual pattern of interferometry when they reach the detector. As a consequence, this quantum transport has an effect on the effective source size observed in HBT measurements. We suggest previously that the multiple scattering in the transport leads to an apparent source that is close to the original chaotic source before the pair quantum transport, supplemented by absorptions along the particle paths [17, 18, 19, 20]. In order to exhibit the importance of this effect, we review the path integral treatment of HBT correlation function under quantum transport as discussed earlier in [19].

For definiteness, we consider the HBT interference of a pair of π^+ particles and study first the motion of one of the two identical pions. As the pion propagates from the state of chemical freeze-out to thermal freeze-out, the scattering can be described by short-ranged scalar and vector interactions, $v_{\text{col}}^{(s,v)}(q - q_i)$, where q is the coordinate of the propagating pion and q_i is the coordinate of a medium particle. The propagating pion is also subject to a collective flow which can be described by a long-range density-dependent mean-field scalar and vector interactions, $V_{\text{mf}}^{(s,v)}(q)$, as in similar cases in the dynamics of the nuclear fluid [37]. The Lagrangian for the propagating pion is given by

$$L(q, \dot{q}) = L_{\text{mf}}(q, \dot{q}) + L_{\text{col}}(q, \dot{q}), \quad (20)$$

$$L_{\text{mf}}(q, \dot{q}) = -[m_\pi + V_{\text{mf}}^{(s)}(q)]\sqrt{1 - \dot{\mathbf{q}}^2} + \dot{\mathbf{q}} \cdot \mathbf{V}_{\text{mf}}^{(v)}(q) - V_{\text{mf}}^{0(v)}(q), \quad (21)$$

where

$$L_{\text{col}}(q, \dot{q}) = -V_{\text{col}}^{(s)}(q)\sqrt{1 - \dot{\mathbf{q}}^2} + \dot{\mathbf{q}} \cdot \mathbf{V}_{\text{col}}^{(v)}(q) - V_{\text{col}}^{0(v)}(q), \quad (22)$$

$$V_{\text{col}}^{(s,v)}(q) = \sum_i v_{\text{col}}^{(s,v)}(q - q_i). \quad (23)$$

From the Lagrangian of the propagating pion, one obtains the pion three-momentum,

$$\mathbf{p} = \partial L / \partial \dot{\mathbf{q}} = \gamma[m_\pi + V^{(s)}(q)]\dot{\mathbf{q}} + \mathbf{V}^{(v)}(q), \quad (24)$$

the pion Hamiltonian,

$$H = p^0 = \mathbf{p} \cdot \dot{\mathbf{q}} - L = \gamma[m_\pi + V^{(s)}(q)] + V^{0(v)}(q), \quad (25)$$

and the pion mass-shell condition,

$$[p^0 - V^{0(v)}(q)]^2 - [\mathbf{p}^2 - \mathbf{V}^{(v)}(q)]^2 - [m_\pi + V^{(s)}(q)]^2 = 0, \quad (26)$$

where $\gamma = 1/\sqrt{1 - \dot{\mathbf{q}}^2}$ and $V^{(s,v)}(q) = V_{\text{mf}}^{(s,v)}(q) + V_{\text{col}}^{(s,v)}(q)$. For a pion produced at x with momentum κ to propagate in the medium to the thermal freeze-out point x_f and be detected at the detecting point x_d with momentum k , the probability amplitude according to the path-integral method is [38, 39]

$$K(\kappa x \rightarrow k x_d) = \int \mathcal{D}q e^{iS(\kappa x \rightarrow k x_d; q)}, \quad (27)$$

where $\int \mathcal{D}q \dots$ is the sum over all paths q from x to x_d , and the action $S(\kappa x \rightarrow k x_d; q)$ is

$$S(\kappa x \rightarrow k x_d; q) = \int L(q, \dot{\mathbf{q}}) dt = - \int_x^{x_d, (\text{path } q)} p(q') \cdot dq'. \quad (28)$$

We can separate $S(\kappa x \rightarrow k x_d; q)$ into different contributions,

$$S(\kappa x \rightarrow k x_d; q) = -k \cdot (x_d - x) + \delta_{\text{mf}}(\kappa x, k x_d; q) + \delta_{\text{col}}(\kappa x, k x_d; q), \quad (29)$$

where

$$\delta_{\text{mf}}(\kappa x, k x_d; q) = - \int_x^{x_d, (\text{path } q)} [p_{\text{mf}}(q') - k] \cdot dq' = - \int_x^{x_f, (\text{path } q)} [p_{\text{mf}}(q') - k] \cdot dq', \quad (30)$$

$$\delta_{\text{col}}(\kappa x, k x_d; q) = - \int_x^{x_d, (\text{path } q)} p_{\text{col}}(q') \cdot dq' = - \int_x^{x_f, (\text{path } q)} p_{\text{col}}(q') \cdot dq', \quad (31)$$

$$p_{\text{mf}}(q) = \left(\gamma[m_\pi + V_{\text{mf}}^{(s)}(q)] + V_{\text{mf}}^{0(v)}(q), \quad \gamma[m_\pi + V_{\text{mf}}(q)]\dot{\mathbf{q}} + \mathbf{V}_{\text{mf}}^{(v)}(q) \right), \quad (32)$$

$$p_{\text{col}}(q) = \left(\gamma V_{\text{col}}^{(s)}(q) + V_{\text{col}}^{0(v)}(q), \quad \gamma V_{\text{col}}^{(s)}(q)\dot{\mathbf{q}} + \mathbf{V}_{\text{col}}^{(v)}(q) \right). \quad (33)$$

Because of the additivity of the collision potentials in Eq. (23), the phase shift for multiple collision δ_{col} is a sum of the phase shifts for individual collisions, similar to the case of the Glauber wave function in multiple scattering [17],

$$\delta_{\text{col}}(\kappa x, k x_d; q) = \sum_i \delta_{\text{col},i}(\kappa x, k x_d; q), \quad (34)$$

where $\delta_{\text{col},i}(\kappa x, k x_d; q)$ is obtained from Eqs. (31) and (33) with the potential $v_{\text{col}}(q - q_i)$ in place of the total collision potential $V_{\text{col}}(q)$. The propagation amplitude is therefore

$$K(\kappa x \rightarrow k x_d) = \int \mathcal{D}q \exp\{-ik \cdot (x_d - x) + i\delta_{\text{mf}}(\kappa x, k x_d; q) + i\delta_{\text{col}}(\kappa x, k x_d; q)\}. \quad (35)$$

In this sum over all possible path q in the above equation, we can make the approximation that the dominant contribution to the path integral comes from the trajectory along the classical path q_c for mean-field motion, as other trajectories give fluctuating contributions that tend to cancel each other. Then the amplitude is approximately

$$K(\kappa x \rightarrow k x_d) \approx \exp\{-ik \cdot (x_d - x) + i\delta_{\text{mf}}(\kappa x, k x_d; q_c) + i\delta_{\text{col}}(\kappa x, k x_d; q_c)\}. \quad (36)$$

It is important to point out that the trajectory in the path integral method is quite general and does not need to follow a straight line. Our previous consideration for the propagation of an energetic pion along a straight-line trajectory in Ref. [17] is just a special case of the path-integral method.

The wave amplitude for the pion to propagate from x to x_d is

$$\Psi(\kappa x \rightarrow k x_d) = A(\kappa x) e^{i\phi_0(x)} K(\kappa x \rightarrow k x_d), \quad (37)$$

where $A(\kappa x)$ is the production amplitude, $\phi_0(x)$ is a random production phase for chaotic source.

The probability amplitude for the production of two identical pions (κ_1, κ_2) at (x_1, x_2) to be detected subsequently as k_1 at x_{d1} and k_2 at x_{d2} is

$$\frac{1}{\sqrt{2}} \left\{ \Psi_1(\kappa_1 x_1 \rightarrow k_1 x_{d1}) \Psi_1(\kappa_2 x_2 \rightarrow k_2 x_{d2}) + (x_1 \leftrightarrow x_2) \right\}, \quad (38)$$

where $(x_1 \leftrightarrow x_2)$ represents the term symmetric to the former by exchanging x_1 and x_2 . The probability $P(k_1, k_2)$ for the detection of two pions with momenta (k_1, k_2) is the absolute square of the sum of the two particle amplitudes (Eq. (38)) from all x_1 and x_2 source points. Because of the random and fluctuating phase $\phi_0(x_i)$ for a chaotic source, the absolute square of the sum of the amplitudes becomes the sum of the absolute squares of the amplitudes [1]. One obtains

$$P(k_1, k_2) = P(k_1)P(k_2) [1 + R(k_1 k_2)], \quad (39)$$

where $P(k)$ is the probability of detecting one pion of momentum k ,

$$P(k) = \sum_x |A^2(\kappa x) K(\kappa x \rightarrow k x_d)|^2 = \sum_x e^{-2\mathcal{I}m \delta_{\text{col}}(\kappa x, k x_d; q_c)} A^2(\kappa x), \quad (40)$$

$$P(k_1)P(k_2)R(k_1 k_2) = \sum_{x_1 x_2} A(\kappa_1 x_1) A(\kappa_2 x_2) K(\kappa_1 x_1 \rightarrow k_1 x_{d1}) K(\kappa_2 x_2 \rightarrow k_2 x_{d2}) \\ \times A(\kappa_1 x_2) A(\kappa_2 x_1) K^*(\kappa_1 x_2 \rightarrow k_1 x_{d1}) K^*(\kappa_2 x_1 \rightarrow k_2 x_{d2}). \quad (41)$$

We can evaluate the product $K(\kappa_1 x_1 \rightarrow k_1 x_{d1}) K^*(\kappa_2 x_1 \rightarrow k_2 x_{d2})$. It is equal to

$$K(\kappa_1 x_1 \rightarrow k_1 x_{d1}) K^*(\kappa_2 x_1 \rightarrow k_2 x_{d2}) = e^{-ik_1 \cdot (x_{d1} - x_1) + ik_2 \cdot (x_{d2} - x_2)} \\ \times \int \mathcal{D}q \int \mathcal{D}q' \exp\{i\delta_{\text{mf}}(\kappa_1 x_1, k_1 x_{d1}; q) - i\delta_{\text{mf}}^*(\kappa_2 x_1, k_2 x_{d2}; q') \\ + i\delta_{\text{col}}(\kappa_1 x_1, k_1 x_{d1}; q) - i\delta_{\text{col}}^*(\kappa_2 x_1, k_2 x_{d2}; q')\}. \quad (42)$$

The real part of the phase difference $\delta_{\text{col}}(\kappa_1 x_1, k_1 x_{d1}; q) - \delta_{\text{col}}^*(\kappa_2 x_1, k_2 x_{d2}; q')$ is stationary when the trajectories q and q' inside the medium coincide and is random and fluctuating when their trajectory in the medium q differs from q' . Thus, we have

$$\int \mathcal{D}q \int \mathcal{D}q' \exp\{i\delta_{\text{mf}}(\kappa_1 x_1, k_1 x_{d1}; q) - i\delta_{\text{mf}}^*(\kappa_2 x_1, k_2 x_{d2}; q') \\ + i\delta_{\text{col}}(\kappa_1 x_1, k_1 x_{d1}; q) - i\delta_{\text{col}}^*(\kappa_2 x_1, k_2 x_{d2}; q')\} \\ \sim \int \mathcal{D}q \exp\{i\delta_{\text{mf}}(\kappa_1 x_1, k_1 x_{d1}; q) - i\delta_{\text{mf}}^*(\kappa_2 x_1, k_2 x_{d2}; q) \\ + i\delta_{\text{col}}(\kappa_1 x_1, k_1 x_{d1}; q) - i\delta_{\text{col}}^*(\kappa_2 x_1, k_2 x_{d2}; q)\}. \quad (43)$$

Among all trajectories inside the medium, the dominant contribution to the path integral comes from those along classical paths,

$$\int \mathcal{D}q \exp\{i\delta_{\text{mf}}(\kappa_1 x_1, k_1 x_{d1}; q) - i\delta_{\text{mf}}^*(\kappa_2 x_1, k_2 x_{d2}; q) \\ + i\delta_{\text{col}}(\kappa_1 x_1, k_1 x_{d1}; q) - i\delta_{\text{col}}^*(\kappa_2 x_1, k_2 x_{d2}; q)\} \\ \sim \exp\{i\delta_{\text{mf}}(\kappa_1 x_1, k_1 x_{d1}; q_c) - i\delta_{\text{mf}}^*(\kappa_2 x_1, k_2 x_{d2}; q_c) \\ + i\delta_{\text{col}}(\kappa_1 x_1, k_1 x_{d1}; q_c) - i\delta_{\text{col}}^*(\kappa_2 x_1, k_2 x_{d2}; q_c)\}. \quad (44)$$

As correlations occur for k_1 close to k_2 these classical paths are close to each other, the real part of the collisional phase shifts approximately cancel and only the additive imaginary part due to absorption remain. We then have

$$i\delta_{\text{col}}(\kappa_1 x_1, k_1 x_{d1}; q_c) - i\delta_{\text{col}}^*(\kappa_2 x_1, k_2 x_{d2}; q_c) \approx -\mathcal{I}m \delta_{\text{col}}(\kappa_1 x_1, k_1 x_{d1}; q_c) - \mathcal{I}m \delta_{\text{col}}(\kappa_2 x_1, k_2 x_{d2}; q_c). \quad (45)$$

The imaginary part of the multiple scattering phase shift $\mathcal{I}m \delta_{\text{col}}(\kappa_1 x_1, k_1 x_{d1}; q_c)$ represents an absorption along the trajectory and can be simplified to be [17, 18, 19, 20]

$$2\mathcal{I}m \delta_{\text{col}}(\kappa_1 x_1, k_1 x_{d1}; q_c) = \int_{x_1}^{x_f, (\text{path } q_c)} n_{\text{med}}(q') \sigma_{\text{abs}} dq', \quad (46)$$

where $n_{\text{med}}(q')$ is the medium density at (q') , σ_{abs} is the pion absorption cross section, and x_f is the freeze-out point. As correlations occur when k_1 is close to k_2 and the absorptions for k_1 and k_2 from x_1 along the trajectory inside the medium are nearly the same, $\mathcal{I}m\delta_{\text{col}}(\kappa_1x_1, k_1x_{d1}; q_c)$ is approximately equal to $\mathcal{I}m\delta_{\text{col}}(\kappa_2x_1, k_2x_{d1}; q_c)$. We can abbreviate these quantities respectively as $\mathcal{I}m\delta_{\text{col}}(k_1, x_1)$ and $\mathcal{I}m\delta_{\text{col}}(k_2, x_1)$ with the other variables implicitly understood.

For the mean-field part of the phase shift, we have

$$\begin{aligned} \delta_{\text{mf}}(\kappa_1x_1, k_1x_{d1}; q_c) - \delta_{\text{mf}}^*(\kappa_2x_1, k_2x_{d2}; q_c) &= \int_{x_1}^{x_f, (\text{path } q_c)} \{[p_{1\text{mf}}(q) - k_1] - [p_{2\text{mf}}^*(q) - k_2]\} \cdot dq \\ &\equiv \phi_{\text{mf}}(k_1k_2, x_1; q_c) \end{aligned} \quad (47)$$

Using $\int d^4x\rho(x)$ to substitute \sum_x in Eqs. (40) and (41) for a continuous pion-emitting source with a density $\rho(x)$, we have

$$P(k) = \int d^4x\rho(x) e^{-2\mathcal{I}m\delta_{\text{col}}(k, x)} A^2(\kappa x), \quad (48)$$

$$P(k_1)P(k_2)R(k_1, k_2) = \int d^4x_1 d^4x_2 \rho(x_1)\rho(x_2) e^{-2\mathcal{I}m\delta_{\text{col}}(k_1, x_1)} e^{-2\mathcal{I}m\delta_{\text{col}}(k_2, x_2)} |\Phi(x_1x_2; k_1k_2)|^2, \quad (49)$$

$$R(k_1, k_2) = \left| \int d^4x e^{i(k_1 - k_2) \cdot x + i\phi_{\text{mf}}(k_1k_2, x; q_c) - \mathcal{I}m\delta_{\text{col}}(k_1, x) - \mathcal{I}m\delta_{\text{col}}(k_2, x)} \rho_{\text{eff}}(k_1k_2, x) \right|^2, \quad (50)$$

where

$$\Phi(x_1x_2; k_1k_2) = \frac{1}{\sqrt{2}} \left\{ \bar{A}(x_1, \kappa_1k_1) \bar{A}(x_2, \kappa_2k_2) e^{ik_1 \cdot x_1 + ik_2 \cdot x_2} + (x_1 \leftrightarrow x_2) \right\}, \quad (51)$$

$$\bar{A}(x, \kappa k) = A(\kappa x) e^{i\delta_{\text{mf}}(\kappa x \rightarrow kx_f; q_c)}, \quad (52)$$

$$\rho_{\text{eff}}(k_1k_2, x) = \frac{\sqrt{f(\kappa_1x)f(\kappa_2x)}}{P(k_1)P(k_2)}, \quad (53)$$

and $f(\kappa x) = \rho(x)A^2(\kappa x)$ is the pion-emitting function of the chaotic source at x with momentum κ that evolves asymptotically to k [17]. We obtain the simple result that the multiple scattering of the interfering pair leads essentially to a factor containing the imaginary part of the phase shift, which is related to the absorption of the particles through the medium [17, 18, 19, 20]. Thus, even though the source expands to a greater spatial dimension during the late stage from chemical freeze-out to thermal freeze-out, the initial chaotic source at chemical freeze-out remains an important element in determining the pair correlation function.

We shall calculate the absorption factor in subsections IIIC and discuss its effect on HBT results in subsection IIID. The collective flow (mean-field interaction) ‘distorts’ the initial momentum κ into the final detected momentum k . The phase associated with the collective expansion of the source, $\phi_{\text{mf}}(k_1k_2, x; q_c)$, is very small [17]. Our calculations indicate that its effect on HBT results can be neglected.

B. Pion-emitting sources

In our model calculations for the two-pion HBT correlation functions, the identical pions (for example π^+) are assumed to be emitted thermally from the space-time hypersurface at T^{ch} for CFO production and from the hypersurface at T^{th} for TFO production. For PCE case, the identical pions includes primary pions produced at the chemical freeze-out (CFO production) as well as secondary pions arising from decay products of excited-state particles during the chemical freeze-out to thermal freeze-out. The four-dimension density of the pion source for PCE production can be written as

$$\rho(x) = n_\pi(x)\delta(\tau - \tau^{\text{ch}}) + \sum_{j \neq \pi} D_{j \rightarrow \pi} n_j(x), \quad (54)$$

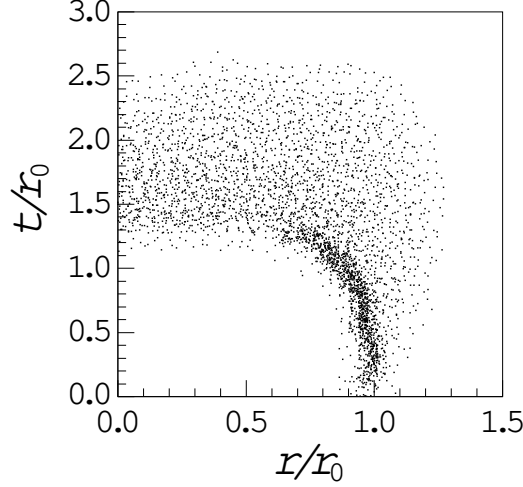


FIG. 2: Space-time distribution of the pion-emitting source for PCE production at AGS energies.

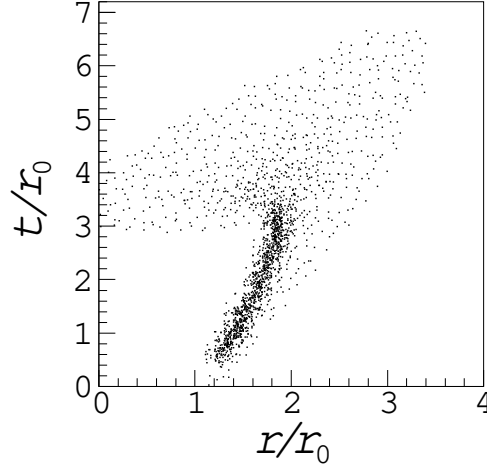


FIG. 3: Space-time distribution of the pion-emitting source for PCE production at RHIC energy.

where τ^{ch} is the chemical freeze-out time in local frame and $D_{j \rightarrow \pi}$ is the decay rate Γ_j times its corresponding fraction $\tilde{d}_{j \rightarrow \pi}$. For example, $D_{\Delta \rightarrow \pi} = \Gamma_{\Delta} \times \frac{1}{3}$, $D_{\rho \rightarrow \pi} = \Gamma_{\rho} \times \frac{2}{3}$, $D_{\omega \rightarrow \pi} = \Gamma_{\omega} \times 0.88$, and $D_{\pi^0 \pi^0 \rightarrow \pi^+ \pi^-} = v_r n_{\pi} \sigma(\pi^0 \pi^0 \rightarrow \pi^+ \pi^-) \times 1$, where v_r is the relative velocity of the two colliding pions. In our calculations, the values of Γ_{Δ} , Γ_{ρ} , and Γ_{ω} are taken as 120 MeV, 145 MeV, and 8 MeV [41]. The cross section $\sigma(\pi^0 \pi^0 \rightarrow \pi^+ \pi^-)$ is equal to the absorption cross section, $\sigma_{\text{abs}}(\pi^+ \pi^- \rightarrow \pi^0 \pi^0)$, and will be discussed in the next subsection.

Fig. 2 shows the space-time distribution of the pion-emitting source in our calculations for the PCE production at AGS energies. Fig. 3 shows the space-time distribution of the pion-emitting source for the PCE particle production at RHIC energy. The produced primary pion source points are distributed near the center of the source and the decay product secondary pion source points are distributed in the outer region of the source. One can see that the space-time geometry of the sources produced at AGS and RHIC energies are different.

C. Cross sections of pion absorption

For the PCE case, the pions propagating in the source during the chemical freeze-out to the thermal freeze-out will subject to multiple scattering with the medium particles in the source. Based on Glauber multiple scattering theory

[40], the absorption factor owing to multiple scattering in Eqs. (48) and (49) can be written as [17, 18, 19, 20]

$$e^{-2\mathcal{I}m \delta_{\text{col}}(x,k)} = \exp \left[- \int_x^{x_f} \sum_i' \sigma_{\text{abs}}(\pi i) n_i(q_c) d\ell(q_c) \right], \quad (55)$$

where \sum_i' means the summation for all particles in the source except for the test pion, $\sigma_{\text{abs}}(\pi i)$ is the absorption cross section of the pion with the medium particle i , and $n_i(q_c)$ is the density of the medium particle i along the classical propagation path q_c .

For the source produced at RHIC energy, pions are the dominant component of produced particles. The other produced particles considered in our model are K , η , ρ , and ω . Because the threshold of the reaction $\pi\pi \rightarrow K\bar{K}$ is greater than $\langle \sqrt{s_{\pi\pi}} \rangle$ in the source and the probability of three-pion collision for $\pi\pi\pi \rightarrow \omega$ is very small, the dominant contributions for the multiple scattering absorption are from reactions $\pi^+\pi \rightarrow \rho$ and $\pi^+\pi^- \rightarrow \pi^0\pi^0$. In our model, the cross sections for the reactions $\pi^+\pi \rightarrow \rho$ and $\pi^+\pi^- \rightarrow \pi^0$ are calculated by [42, 43]

$$\sigma_{\text{abs}}(\pi^+\pi \rightarrow \rho) = \frac{4\pi}{p_{\text{cm}}^2} \sin^2 \delta_1 \quad (56)$$

and

$$\sigma_{\text{abs}}(\pi^+\pi^- \rightarrow \pi^0\pi^0) = \frac{8}{9} \frac{\pi}{p_{\text{cm}}^2} \sin^2(\delta_0 - \delta_2), \quad (57)$$

where $p_{\text{cm}} = \sqrt{s_{\pi\pi} - 4m_\pi^2}/2$ and the phase shifts δ_0 , δ_1 , and δ_2 are given by Ref. [43].

For the source produced at AGS energies, the dominant contribution for the multiple scattering absorption is from the process $\pi^+N \rightarrow \Delta$. We calculate the absorption cross section in our model by

$$\sigma_{\text{abs}}(\pi^+N \rightarrow \Delta) = \frac{2}{3} \frac{\sigma_0 (\Gamma_\Delta/2)^2}{(\sqrt{s_{\pi N}} - m_\Delta)^2 + (\Gamma_\Delta/2)^2}, \quad (58)$$

where $m_\Delta = 1232$ MeV and $\sigma_0 = 200$ mb.

D. Calculation of $P(k)$ and $P(k_1, k_2)$

After knowing the hydrodynamical solution, we have the space-time distributions of temperature, chemical potential, and velocity of the evolving source. Then, we can calculate $P(k)$ and $P(k_1, k_2)$ for constructing HBT correlation function based on Eqs. (48) and (49) in the following steps:

Step 1: Select space-time coordinate of the first test pion, x_1 , in the source randomly with the probability of the space-time source density $\rho(x)$ (at $T^{\text{ch}} < T < T^{\text{th}}$, see Figs. 2 and 3).

Step 2: Generate the momentum of the pion in local frame, $\kappa'_1 = (E'_1, \boldsymbol{\kappa}'_1)$, according to the Bose-Einstein distributions at the point x_1 , which is a function of the temperature and chemical potential at x_1 .

Step 3: Boost κ'_1 by the Lorentz transform with the source fluid velocity at x_1 . Then, we get the momentum of the pion in the center of mass frame of the source, $\kappa_1 = (E_2, \boldsymbol{\kappa}_1)$.

Step 4: Determine the new space coordinate of the pion propagating along classical path at next time by the production of the pion's velocity $\boldsymbol{\beta}_1 = \boldsymbol{\kappa}_1/E_1$ and the step of time Δt . If the temperature at the new point is higher than T^{ch} we re-select the pion from step 1 to step 3.

Step 5: Boost κ'_1 by the Lorentz transform with the source velocity at the new point to get the momenta of the pion at the point and calculate $w_{\text{ms1}} = \sum_j \sigma_{\text{abs}}(\pi j) n_j \sqrt{(\boldsymbol{\beta}_1 \Delta t)^2}$ at this new point.

Step 6: Repeat steps 4 and 5 until the point x_f at the temperature T^{th} to get the final (detected) momentum of the pion, k_1 , and accumulate w_{ms1} to get the values of $e^{-2\mathcal{I}m \delta_{\text{col}}(x_1, k_1)}$ based on Eq. (55).

Step 7: Repeat step 1 to step 6 to get the corresponding quantities for the second test pion.

Step 8: According to Eqs. (48) and (49) calculate the weights

$$W_i = e^{-2\mathcal{I}m \delta_{\text{col}}(x_i, k_i)} [E'_i/E_i(\mathbf{k}_i)], \quad i = 1, 2 \quad (59)$$

and

$$\begin{aligned} W_{12} &= e^{-2\mathcal{I}m \delta_{\text{col}}(x_1, k_1)} e^{-2\mathcal{I}m \delta_{\text{col}}(x_2, k_2)} \frac{1}{2} \left| \sqrt{E'_1/E_1} \sqrt{E'_2/E_2} \right. \\ &\quad \left. \times e^{ik_1 \cdot x_1 + ik_2 \cdot x_2} + \sqrt{E'_{12}/E_1} \sqrt{E'_{21}/E_2} e^{ik_1 \cdot x_2 + ik_2 \cdot x_1} \right|^2 \end{aligned} \quad (60)$$

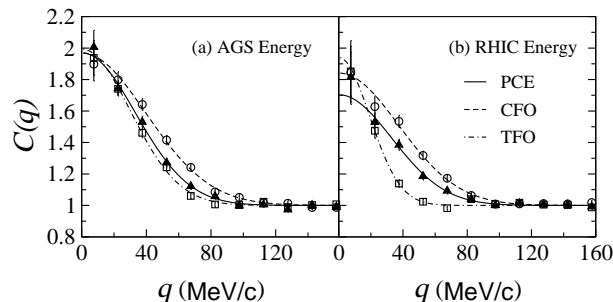


FIG. 4: The two-pion correlation functions for the sources produced at AGS and RHIC energies.

for $P(k_i)$ ($i = 1, 2$) and $P(k_1, k_2)$, where E'_{ij} ($i, j = 1, 2$) is the energy of the i th pion in the local frame at x_j , which is obtained from E_i by a reverse Lorentz transformation with the source velocity at x_j .

Step 9: Repeat step 1 to step 8 and accumulate W_i ($i = 1, 2$) and W_{12} for each $(\mathbf{k}_1, \mathbf{k}_2)$ bin, respectively. Then we get the one-pion and two-pion momentum distributions $P(k)$ and $P(k_1, k_2)$ for constructing HBT correlation functions.

E. HBT results

The two-particle HBT correlation function $C(k_1, k_2)$ is defined as the ratio of the two-pion momentum distribution $P(k_1, k_2)$ to the the product of the single-pion momentum distribution $P(k_1)P(k_2)$,

$$C(k_1, k_2) = \frac{P(k_1, k_2)}{P(k_1)P(k_2)}. \quad (61)$$

Using the relative momentum of the two selected pions, $q = |\mathbf{k}_1 - \mathbf{k}_2|$, as variable, we construct the two-pion correlation function $C(q)$ from $P(k_1, k_2)$ and $P(k_1)P(k_2)$ by picking the identical pion pairs emitted from the source and summing over \mathbf{k}_1 and \mathbf{k}_2 for each q bin [20, 44]. Fig. 4 (a) and (b) show the two-pion correlation functions for sources produced at AGS and RHIC energies, respectively. In Fig. 4, the symbols circle and up-triangle symbols are the results for the CFO and PCE particle productions. The square symbols present the results for the TFO particle production, for this case the HBT calculations of quantum path-integral reduce to a usual HBT calculation for a certain source configuration. The curves in Fig. 4 are obtained by fitting the model calculation data of the two-pion correlation functions with the parametrized formula

$$C(q) = 1 + \lambda e^{-q^2 R^2}. \quad (62)$$

Table 1 gives the fitted HBT radii R and chaotic parameter λ in this parametrized formula. In our model calculations, the initial source radius, r_0 , is taken as 6 fm both for the sources produced at AGS and RHIC energies. We can see that the HBT radii for the CFO and PCE productions are obviously smaller than those for the TFO particle production, especially at RHIC energy. This arises because that the thermal freeze-out is the latest states of the expanding sources, which have the largest space geometry of the sources, and at RHIC energy the expanding velocity is higher. In order to investigate the effects of the excited-state particle decays and multiple scattering absorption on the HBT results in the PCE case, we also examine the HBT correlation functions without the multiple-scattering absorptions by letting the absorption factor equal to 1. The corresponding HBT results are listed on right column of Table 1. One can see that the HBT radii for the PCE without multiple-scattering absorptions case are larger than those for the CFO case because of the excited-state particle decays. The multiple scattering of the identical pions with the medium particles in the source leads to an absorption factor to the source density for calculating the two-pion HBT correlation functions. It constrains the pions produced near the center of the source and leads to a larger space configuration of the pion-emitting source.

By comparing the HBT radii for the PCE case with and without absorption for the source produced at AGS energies, Table 1 indicates that the effect of the large absorption by delta formation increases the HBT radius, as the source of pions are located farther out in the expanding system. On the other hand, the HBT radius for the PCE case is close to that for the PCE case without absorption, for collisions at RHIC energies. This indicates that for RHIC collisions, the effects of absorption is small because the cross sections for $\pi^+\pi^- \rightarrow \pi^0\pi^0$ and $\pi\pi \rightarrow \rho$ are small. Our results show that at RHIC energy the values of λ for the CFO and PCE cases are smaller than unit even for the

TABLE I: The HBT fitted results (the unit of source radii R is fm).

	PCE	CFO	TFO	PCE non-abs.
AGS	$R = 4.20 \pm 0.15$ $\lambda = 0.97 \pm 0.05$	$R = 3.51 \pm 0.11$ $\lambda = 0.97 \pm 0.05$	$R = 4.64 \pm 0.16$ $\lambda = 0.99 \pm 0.06$	$R = 3.79 \pm 0.13$ $\lambda = 0.98 \pm 0.05$
RHIC	$R = 4.22 \pm 0.23$ $\lambda = 0.70 \pm 0.06$	$R = 3.74 \pm 0.15$ $\lambda = 0.84 \pm 0.06$	$R = 7.28 \pm 0.42$ $\lambda = 0.94 \pm 0.12$	$R = 4.44 \pm 0.23$ $\lambda = 0.79 \pm 0.07$

chaotic sources we consider in the paper. Investigating the reason of the λ results will be of interest in our future work.

IV. SUMMARY AND DISCUSSION

Quantum transport of the pair of interfering pion pair has an important influence in the properties of HBT interferometry in heavy-ion collisions. Starting with a chaotic source at chemical freeze-out, we examine the effects of this quantum transport using the path integral method, in which the evolution of the bulk matter is described by relativistic hydrodynamics while the paths of the two interfering pions are described by test particles following the hydrodynamical fluid positions and velocity fields. By following the trajectories of the interfering pion pair after chemical freeze-out up to thermal freeze-out, we find that the quantum transport leads to a cancellation of the real part of the phase shifts but the imaginary part leads to an absorption of the propagating pions. The transport gives rise to an a HBT radius closer to the radius at chemical freeze-out. We examine in addition the effects of particle decay from which secondary pions are produced after chemical freeze-out. As the system continue to expand after chemical freeze-out, the spatial dimension of the secondary pions are greater than those of the chemical freeze-out source. Secondary pions will lead to a greater HBT radius. The combined effects of of multiple scattering and excited-state particle decays lead to HBT radii for the PCE case larger than those for the CFO case, but smaller than those of the TFO case.

The nature of the particle-emitting sources produced in high energy heavy ion collisions at RHIC energy is different from that produced in the collisions at AGS energies. At AGS energies, the sources may be described by mixed hadronic gas with finite baryon densities. The main stable particles in the sources are nucleons and produced pions, and the main excited-state particle may be considered to be $\Delta(1232)$. Whereas at RHIC energies, the sources undergo a phase transition from the quark-gluon plasma (QGP) phase to the hadronic gas phase, and with an approximate zero baryon density. The main stable particles are produced pions and kaons, and there are many excited-state particles, such as ρ and ω in the sources. At AGS energies this effect increases the HBT radius for the PCE case to be substantially larger than the HBT radius for the CFO case. Whereas at RHIC energies, the HBT radius for the PCE case increases only slightly from the CFO value and is about the same as the PCE case without absorption, because the absorption cross sections are small.

In our calculations we consider only the spherical evolving sources for simplicity. In high-energy heavy-ion collisions, the evolution of the system is different in the longitudinal direction (beam direction) and the transverse direction. This effect is important for sources produced at RHIC energies. Therefore, it will be of great interest to examine the HBT interferometry with quantum transport of the interfering pion pair for more reasonable evolving source models and investigate the HBT radii in different directions (“out”, “side”, and “long” directions) in the future.

Acknowledgments

This research was supported by the National Natural Science Foundation of China under Contract Nos. 10575024 and 10775024 and in part by the Division of Nuclear Physics, US DOE, under Contract No. DE-AC05-00OR22725 managed by UT-Battle, LC.

-
- [1] C. Y. Wong, *Introduction to High-Energy Heavy-Ion Collisions* (World Scientific, Singapore, 1994), Chap. 17.
 - [2] U. A. Wiedemann and U. Heinz, Phys. Rept. **319**, 145 (1999).
 - [3] R. M. Weiner, Phys. Rept. **327**, 249 (2000).
 - [4] M. A. Lisa, S. Pratt, R. Soltz, U. Wiedemann, Ann. Rev. Nucl. Part. Sci. 55, 357 (2005); nucl-ex/0505014.

- [5] R. J. Glauber, Phys. Rev. Lett. **10**, 84 (1963); R. J. Glauber, Phys. Rev. **130**, 2529 (1963); R. J. Glauber, Phys. Rev. **130**, 2766 (1963).
- [6] E895 Collaboration, M. A. Lisa *et al.*, Phys. Rev. Lett. **84**, 2789 (2000).
- [7] WA98 Collaboration, M. M. Aggarwal *et al.*, Eur. Phys. J. **C16**, 445 (2000).
- [8] NA44 Collaboration, I. G. Beardden *et al.*, Eur. Phys. J. **C18**, 317 (2000).
- [9] E802 Collaboration, L. Ahle *et al.*, Phys. Rev. C **66**, 054906 (2002).
- [10] STAR Collaboration, C. Adler *et al.*, Phys. Rev. Lett. **87**, 082301 (2001).
- [11] PHENIX Collaboration, K. Adcox *et al.*, Phys. Rev. Lett. **88**, 192302 (2002).
- [12] PHENIX Collaboration, S. S. Adler *et al.*, Phys. Rev. Lett. **93**, 152302 (2004).
- [13] STAR Collaboration, J. Adams *et al.*, Phys. Rev. C **71**, 044906 (2005).
- [14] T. Hirano, K. Tsuda, Phys. Rev. C **66**, 054905 (2002).
- [15] E. V. Shuryak, Nucl. Phys. A **661**, 119 (1999).
- [16] U. Heinz, Nucl. Phys. A **661**, 140 (1999).
- [17] C. Y. Wong, J. Phys. G **29**, 2151 (2003).
- [18] C. Y. Wong, J. Phys. G **30**, S1053 (2004).
- [19] C. Y. Wong, AIP Conference Proc. **828**, 617 (2006); hep-ph/0510258.
- [20] W. N. Zhang, M. J. Efaaf, C. Y. Wong, and M. Khaliliasr, Chin. Phys. Lett. **21**, 1918 (2004), hep-ph/0404047.
- [21] J. I. Kapusta and Y. Li, J. Phys. **G30**, S1069 (2004); J. I. Kapusta and Y. Li, Phys. Rev. C **72**, 064902 (2005).
- [22] J. G. Miller, G. A. Cramer, J. M. S. Wu, and J. H. S. Yoon, Phys. Rev. Lett **94**, 102302 (2005); and J. G. Miller and G. A. Cramer, nucl-th/0507004.
- [23] O. Socolowski Jr, F. Grassi, Y. Hama, T. Kodama Phys. Rev. Lett. **93**, 182301 (2004); Y. Hama, R. P.G. Andrade, F. Grassi, O. Socolowski Jr, T. Kodama, B. Tavares, S. S. Padula, Nucl.Phys. A774 (2006) 169 (2004) and arXiv:hep-ph/0510101.
- [24] D. H. Rischke and M. Gyulassy, Nucl. Phys. A **608**, 479 (1996).
- [25] D. H. Rischke, Proceedings of the 11th Chris Engelbrecht Summer School in Theoretical Physics, Cape Town, February 4-13, 1998; nucl-th/9809044.
- [26] P. Kolb and U. Heinz, nucl-th/0305084.
- [27] L. D. Landau and E. M. Lifshitz, *Fluid Mechanics* (Pergamon, New York, 1959).
- [28] V. Schneider *et al.*, J. Comput. Phys. **105**, 92 (1993).
- [29] D. H. Rischke, S. Bernard, and J. A. Maruhn, Nucl. Phys A **595**, 346 (1995).
- [30] G. A. Sod, J. Fluid Mech. **83**, 785 (1977).
- [31] W. N. Zhang, M. J. Efaaf, C. Y. Wong, Phys. Rev. C **70**, 024903 (2004).
- [32] J. P. Blaizot and J. Y. Ollitrault, Phys. Rev. D **36**, 916 (1987).
- [33] E. Laermann, Nucl. Phys. A **610**, 1 (1996).
- [34] A. Chodos, R. L. Jaffe, K. Johnson, C. B. Thorn, and V. F. Weisskopf, Phys. Rev. D **9**, 3471 (1974).
- [35] H. Bebie, P. Gerber, J. L. Goity, and H. Leutwyer, Nucl. Phys. B **378**, 95 (1992).
- [36] J. Cleymans and K. Redlich, Phys. Rev. Lett. **81**, 5284 (1998).
- [37] C. Y. Wong, J. Maruhn, and T. Welton, *Nucl. Phys. A* **253**, 469-489 (1975); C. Y. Wong and H. H. K. Tang, *Phys. Rev. Lett.* **40**, 1070-1073 (1978); C. Y. Wong and H. H. K. Tang, *Phys. Rev.* **20**, 1419-1452 (1979); C. Y. Wong, *Phys. Rev.* **25**, 1460-1475 (1982).
- [38] R. P. Feynman and A. R. Hibbs, *Quantum Mechanics and Path Integrals*, McGraw-Hill Companies, 1965.
- [39] For a recent review on the path-integral method, see H. Kleinert, *Path Integrals in Quantum Mechanics, Statistics, Polymer Physics, and Financial Markets*, World Scientific Pub. Company, Singapore 2004, Fourth Extended Edition.
- [40] R. J. Glauber, in *Lectures in Theoretical Physics*, (Interscience, N.Y., 1959), Vol. 1, p. 315.
- [41] K. Hagiwara *et al.*, Phys. Rev. D **66**, 010001 (2002), available on the PDG WWW pages (URL: <http://pdg.lbl.gov/>).
- [42] B. R. Martin, D. Morgan, and G. Shaw, *Pion-Pion Interaction in Particle Physics*, Academic Press, 1976, p.101.
- [43] F. J. Yndurain, hep-ph/0212282
- [44] W. N. Zhang, Y. M. Liu, S. Wong, Q. J. Liu, J. Jiang, D. Keane, Y. Shao, S. Y. Chu, and S. Y. Feng, Phys. Rev. C **47**, 795 (1993); W. N. Zhang, Y. M. Liu, L. Huo, Y. Z. Jiang, D. Keane, and S. Y. Feng, Phys. Rev. C **51**, 922 (1995); W. N. Zhang, S. X. Li, C. Y. Wong, and M. J. Efaaf, Phys. Rev. C **71**, 064908 (2005).